Three-Dimensional Finite Element Analysis of a Post-tensioned Concrete Containment with Ungrouted Tendons to Inform a Probabilistic Risk Assessment

Hernando Candra[1] and Jose A. Pires[2*]

[1] Sr. Structural Engineer, Division of Engineering, Office of Nuclear Regulatory Research, U.S. Nuclear Regulatory Commission, Rockville, Maryland, United States (Hernando.Candra@nrc.gov)
[2*] Sr. Technical Advisor for Civil/Structural Engineering, Division of Engineering, Office of Nuclear Regulatory Research, U.S. Nuclear Regulatory Commission, Rockville, Maryland, United States (Jose.Pires@nrc.gov)

Introduction

This paper describes the modeling and results of the three-dimensional (3D) finite element analysis of a post-tensioned concrete containment with ungrouted tendons for beyond-design basis internal pressurization. The goals of the analysis are (1) to illustrate results that would inform Level 2 probabilistic risk assessments and (2) to assess modern modeling and analysis techniques. Main results of the analysis are (1) estimates of the internal pressures at which the containment would start to leak as result of liner tears from the internal pressurization and (2) the evolution of the leakage area from liner tearing with increasing internal pressurization. The analysis results also provide an estimate of the failure pressure capacity of the containment as measured by either the pressure at which strains of about 1-percent would be widespread in the hoop tendons [NRC10] or the pressure at which shear failure at the junction of the containment wall to the foundation slab (basemat) might initiate. Internal pressures corresponding to those containment failure pressures are possible only if the rate of internal pressurization from the severe accident exceeds the leakage rate from tearing of the liner. The nonlinear, explicit, finite element code LSDYNA [LST13] was chosen for the analysis to take advantage of its contact modeling features and of the Arbitrary Lagrangian-Eulerian formulation in its constrained Lagrange in solid options. Use of the explicit code also circumvents the need for repeatedly assembling and solving large systems of equations which is expected to be advantageous for the development of fragility information using the Latin Hypercube Sampling and parallelized computing.

Containment Description and Modeling

The containment analyzed consists of a cylindrical wall and a hemispherical dome on a reinforced concrete basemat (see Figure 1 for aspects of the model). The interior diameter,

overall height and cylindrical wall height are approximately 42m (138ft), 69.6m (228ft), and 48.3m (158ft). The containment has three vertical buttresses at 120-degree spacing that extend to the top of the containment dome. Vertical tendons are anchored at the tendon gallery, extend over the dome and are post-tensioned from both ends (at the tendon gallery). Hoop tendons have anchors spaced at 240-degrees to provide tendon overlap, and are post-tensioned from both ends. At a strain of about 1%, the force in the pre-stressing tendons using estimated median material properties is approximately 9.7×10^{6}newtons (2.2×10^{6}lbf). The containment passive steel reinforcing bars (rebars) are also represented in the model including the complex rebar patterns in the basemat, at the buttresses and at the base of the walls. The containment wall is 114cm (45-inch) thick and tapers near the base to a 145cm (57-inch) thickness. At the containment wall the buttresses are 183cm (72-inch) thick and taper at the base to a 214cm (84-inch) thickness. The dome wall is 114cm (45-inch) thick and the basemat slab near the wall-basemat junction is 214cm (126-inch) thick.

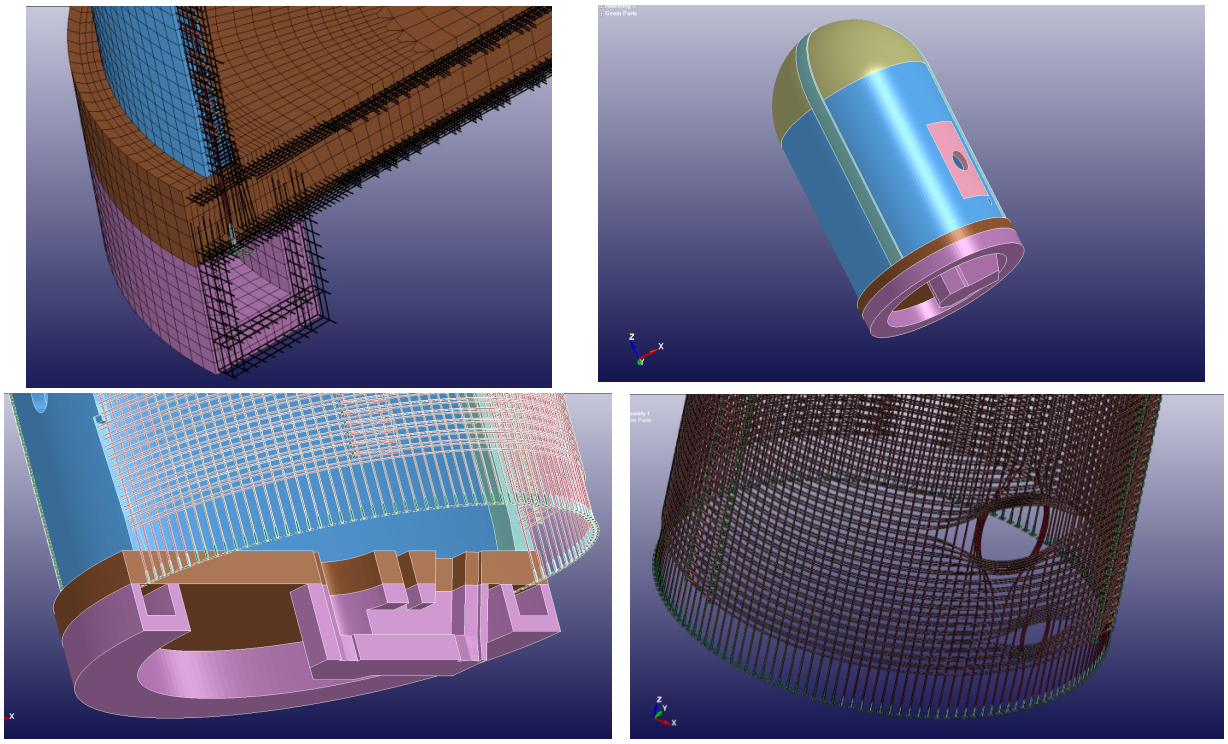

Figure 1: Containment Finite Element Model

The model includes the opening for the containment hatch, the increase in the concrete wall thickness and liner thickness around the equipment hatch as well as a simple representation of the hatch dome and penetration. In addition, the model includes the openings for the personnel access lock and emergency airlock with a representation of the metallic parts of these

penetrations. Table 1 is a summary of the finite elements used to model the containment, the number of elements, and the material models used. All results provided in this paper are median-centered values in the sense that they were obtained using best estimates of the median values of the material properties for the various structural components as shown in Table 2.

Table 1: Finite elements and material models used

Structural Element	**Element Type**	**Number of Elements**	**Material Type**
Concrete	8-noded solid elements with reduced integration	185,558	Winfrith concrete model without strain rate effects (LSDYNA Material 85)
Liner, Hatch and Personal Airlock Domes	4-noded Belytschko-Tsay shell elements	29,132	Elastic-plastic with bilinear kinematic hardening
Reinforcement	LSDYNA beam elements (truss option)	238,809	Same as above
Prestressing Tendons	LSDYNA beam elements (truss option)	54,210	Same as above
Tendon conduits	4-noded Belytschko-Tsay shell elements	350,885	Same as above
Tendon bearing plates	4-noded Belytschko-Tsay shell elements	7,744	Same as above

Table 2: Material properties used in the analysis

Structural Component and Material	Properties (stresses and moduli in MPa)
Tendons (prestressing steel)	Yield stress = 1790; Young's modulus = 187000 Tangent modulus = 4825; Failure Strain = 3.7%
Reinforcing bars steel	Yield stress = 469; Young's modulus = 200000 Tangent modulus = 2080; Failure strain = 7%
Liner steel	Yield Stress = 255; Young's Modulus = 200000 Tangent Modulus = 2782; Failure Strain = 15%
Containment cylinder/dome concrete	Uniaxial compressive stress = 52.6; Tensile stress = 4.5 Small strains modulus = 34320; Crack width = 0.3mm (0.012-inch) Aggregate size = 38mm (1.5-inch) diameter
Basemat concrete	Uniaxial compressive stress = 43.2; Tensile stress = 4.1 Small strains modulus = 31120; Crack width = 0.33mm (0.012-inch) Aggregate size = 38mm (1.5-inch) diameter

Contact Algorithms – The analysis requires a set of contact definitions and related friction modeling properties to calculate the variation of the prestress along the tendons before the

application of the internal pressure loads, and to account for friction between the tendons and the ducts during the pressurization. A critical aspect of the modeling is, therefore, the selection of contact algorithms in LSDYNA to model (1) the contact between the hoop tendons and their sleeves (or conduits), (2) the contact between the vertical tendons and their conduits, (3) the contact between the anchor plates for the hoop tendons and the concrete at the buttresses, and (4) the contact between the anchor plates for the vertical tendons and the concrete at the bottom of the basemat on the ceiling of the tendon gallery. Modeling for this analysis uses the LSDYNA contact algorithm called automatic nodes to surface. The contact definitions use part set identification labels for the contact between the tendons and their sleeves with the sleeves parts as the masters. The contact between the anchor plates and the concrete uses node sets for the anchor plates and master segment sets for the concrete surfaces. Nodes of anchor plates are offset from the concrete wall by a distance equal to half the assumed plate thicknesses. The friction coefficient for the friction between the tendons and their conduits is taken to be equal to 0.25.

Modeling of the reinforcing bars and of the tendon conduits inside the concrete is done using the constrained Lagrange in solid option in LSDYNA. The modeling uses two definitions for these constraints. One definition uses a part set for all parts that represent reinforcing bars with a master part set for all concrete parts. The other definition uses a part set for all parts representing tendon sleeves with a master part set for all concrete parts. While the ducts are modeled as 6-sided hollow conduits embedded in the concrete, the tendons are placed inside these conduits and allowed to interact only with the inside surface of the ducts and the anchor plates.

Analysis

The analysis consisted of the following steps: (1) a dynamic relaxation step for the application of the gravity (dead) loads and initial pre-stressing; and (2) a second step for the application of the internal pressurization, which is applied slowly in order to preclude the development of significant dynamic effects in the explicit analysis. The dynamic relaxation is used to determine the variation of the prestress forces along the tendons as well as the resulting initial stresses in the concrete before application of the internal pressure loads. Initial prestress values are assigned to selected tendon elements at a chosen distance from their anchorage as the starting point for the dynamic relaxation as shown in Figure 2 for a set of vertical tendons and for

the hoop tendons on the cylindrical wall. Forces in those vertical and hoop tendons at the end of the dynamic relaxation are as shown in Figure 3.

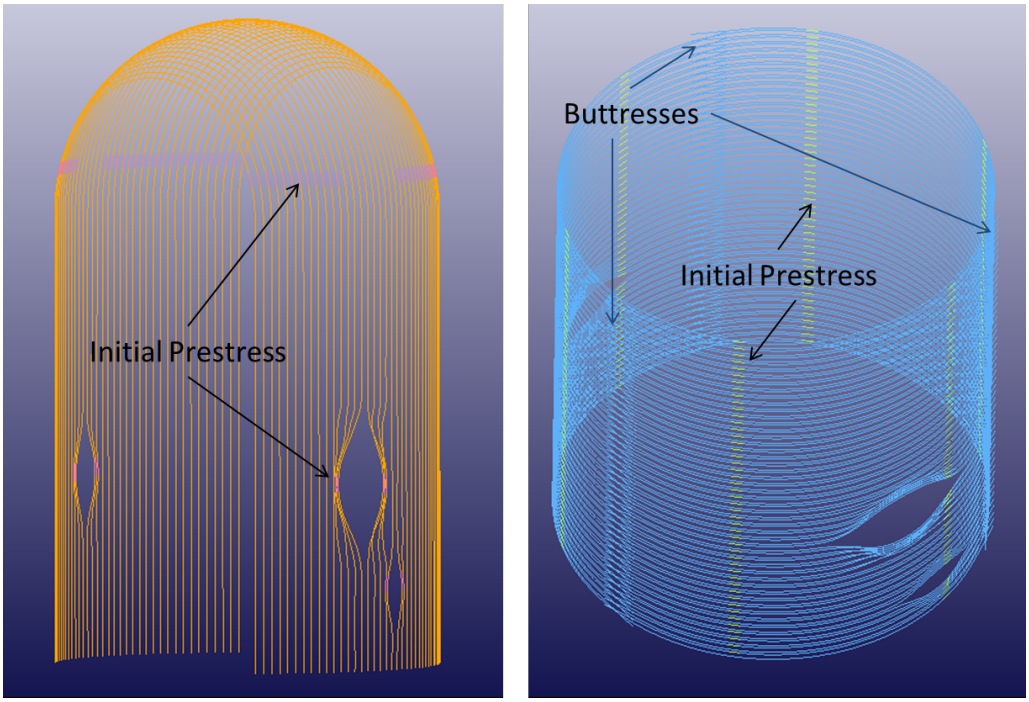

Figure 2: Vertical tendons (left) and hoop tendons in the vertical wall (right) showing location of elements initially stressed for the dynamic relaxation

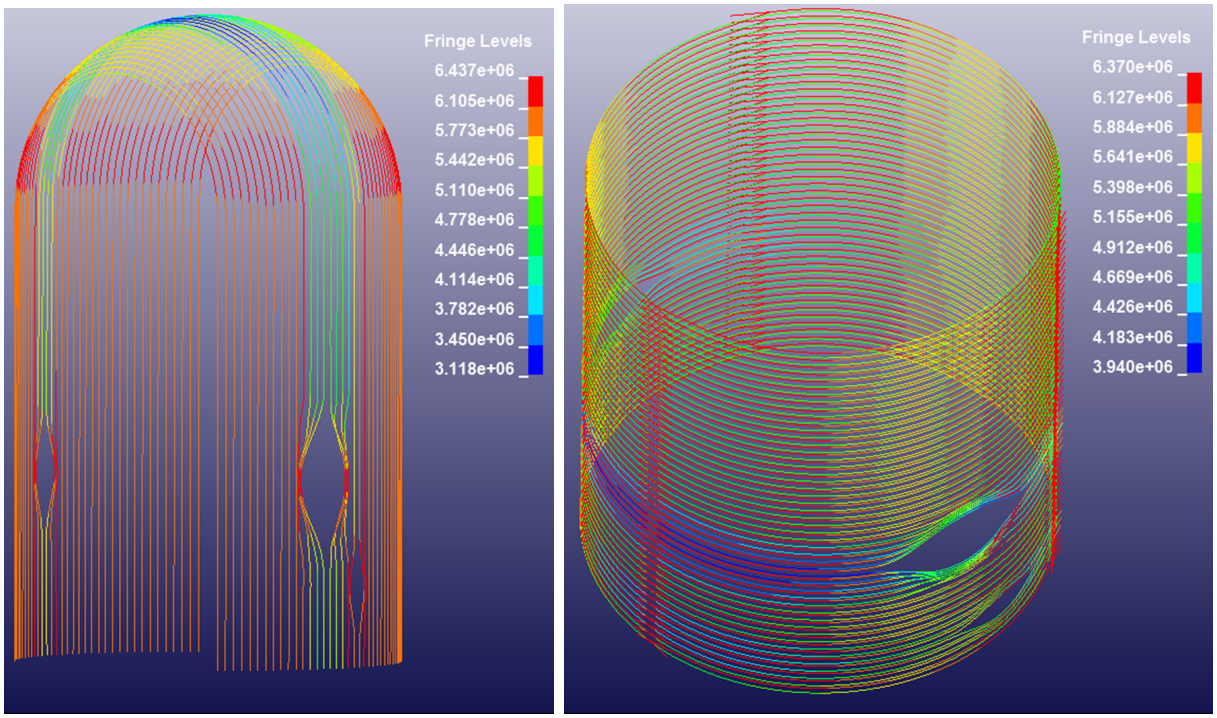

Figure 3: Vertical tendons (left) and hoop tendons in the vertical wall (right) showing forces at the end of the dynamic relaxation (initial force was 6.36×10^{6}newtons (1.43×10^{6}lbf))

The approach to estimate the onset of containment leakage, the expected locations of containment leakage and the increase in the leakage area with pressurization, uses the results of the 3D finite element analysis in conjunction with statistical data for the failure strain of the liner materials (carbon steel) in Cherry (1996) [CHE96], strain concentration factors for liner strains in regions of high strain concentration proposed by Tang et al. (1995) [TAN95] as well as models for the calculation of resulting leakage areas that were used in previous risk studies [SPE06] [PET13]. The size of the elements in the 3D finite element model near the regions of high strain concentration is not sufficiently small to capture the high strain concentrations. Regions of high strain concentration where liner tearing is more likely have been defined in [TAN95] such as the regions near the containment hatch, the wall-basemat junction and the spring line. Strain concentration factors to be applied to the results of less detailed finite element models have been published for these regions in [TAN95] and are used here to obtain the results shown here.

Estimation of the onset of the liner tearing and of leakage areas requires a post-processing approach for the results of the 3D finite element analysis. This approach consists of defining elements in each one of the regions of high strain concentration, retrieving the strains for these elements from the 3D analyses for the direction of interest, multiplying these strains by the strain concentration factors and then comparing the resulting high strains with limiting strains for the liner from Cherry 1996 [CHE96]. The post-processing approach sets a flag for those elements where liner tearing starts. The crack width for these elements is then taken to be the strain on the adjacent wall of the containment multiplied by an estimate of the anchor spacing [CHE01], [PET13]. In this analysis, the estimate of the anchor spacing is taken to be the width of the element in the direction of the strain of interest. The crack area is then the product of the crack width and the other dimension of the element. Although the width of the element is less than the spacing of the anchor, the resulting error in the related internal pressure is expected to be small. This is so because the total leakage area calculated in this manner increases rapidly as a result of the rapid spread of the liner tearing and increase in the strain of the finite element wall.

The analysis uses this approach in conjunction with threshold leak areas (limit states) associated with containment performance as described in [SPE06] and [PET13]. Accordingly, the analysis defines three leakage related limit states for large dry concrete containments as follows: (1) initiation of liner tearing, (2) leakage damage state for a leakage area of about 93cm^2

($0.1ft^2$), and (3) containment functional rupture for leakage areas in the range of 280 cm^2 to 930 cm^2 ($0.3ft^2$ to $1.0ft^2$).

Summary of Results

Table 3 is a summary of the main results of the analysis. The paragraphs that follow Table 3 contain a brief description of the results in the table which addresses how the results are obtained and the interpretation of those results for possible use in a Level 2 PRA.

Table 3: Summary of the Analysis Results

Limit State	**Internal Pressure (MPa) (psig in parentheses)**	
	Equipment Hatch, Emergency Airlock and Personal Airlock	Wall-Basemat Junction
Initiation of Liner Tearing	0.83 (120)	0.88 (128)
Leakage Area ≈ $93cm^2$ ($0.1ft^2$)	0.86 (124)	0.90 (131)
Leakage area 280 cm^2 – $930cm^2$ ($0.3ft^2$ – $1.0ft^2$)	0.87 - 0.88 (126 – 128)	0.90 – 0.92 (131 – 134)
Containment Failure: 1% hoop tendon strain	1.10 – 1.16 (159 – 168)	N/A
Containment Failure: wall-basemat shear	N/A	1.16 – 1.20 (168 – 174)

Initiation of Liner Tearing – Using estimates for the median values of the material properties, the method for the calculation of liner tearing used in previous risk studies [CHE96] [CHE01], [PET13], and strain concentration factors in [TAN95], the results of the analysis indicate that liner tearing and related containment leakage would start at about 0.83 MPa (120psig) near the containment hatch, at the emergency airlock below the containment hatch and at the personal access hatch (see Figure 4 for these locations). In the region near the equipment hatch, liner tearing and related leakage would be expected along the two vertical lines where both the containment wall and liner thickness increase to strengthen the containment wall near the hatch. The analysis also indicates that liner tearing and related containment leakage would start at the junction of the containment wall to the basemat at internal pressures of about 0.88MPa (128psig) (see Figure 5 for these locations).

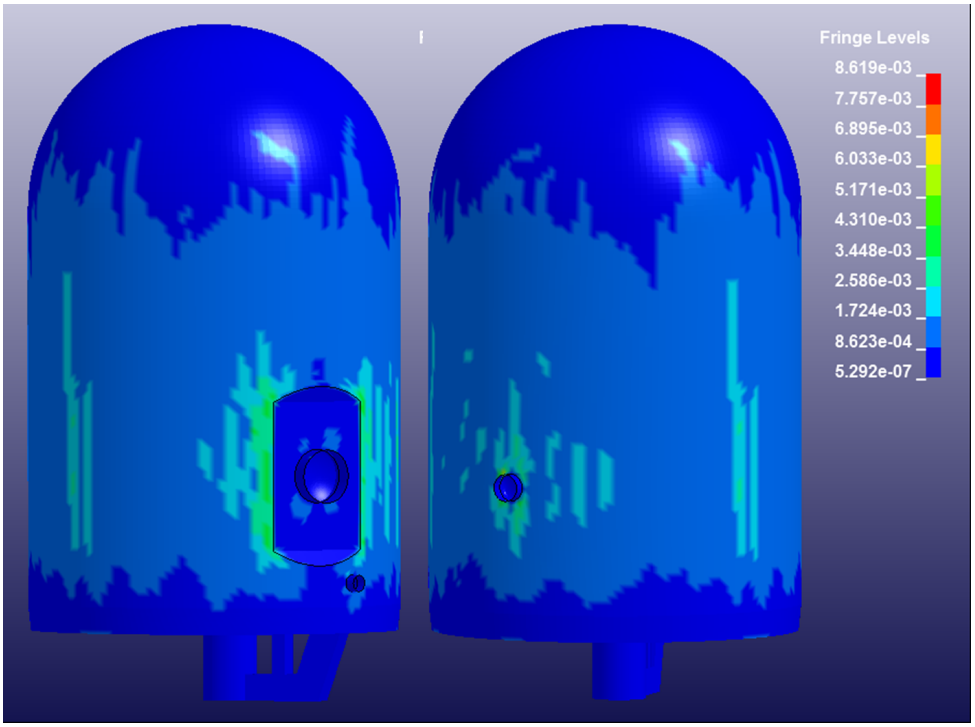

Figure 4: Maximum principal strains at 0.86MPa (124psig) in the liner at the equipment hatch and emergency airlock (left) and personnel access hatch (right)

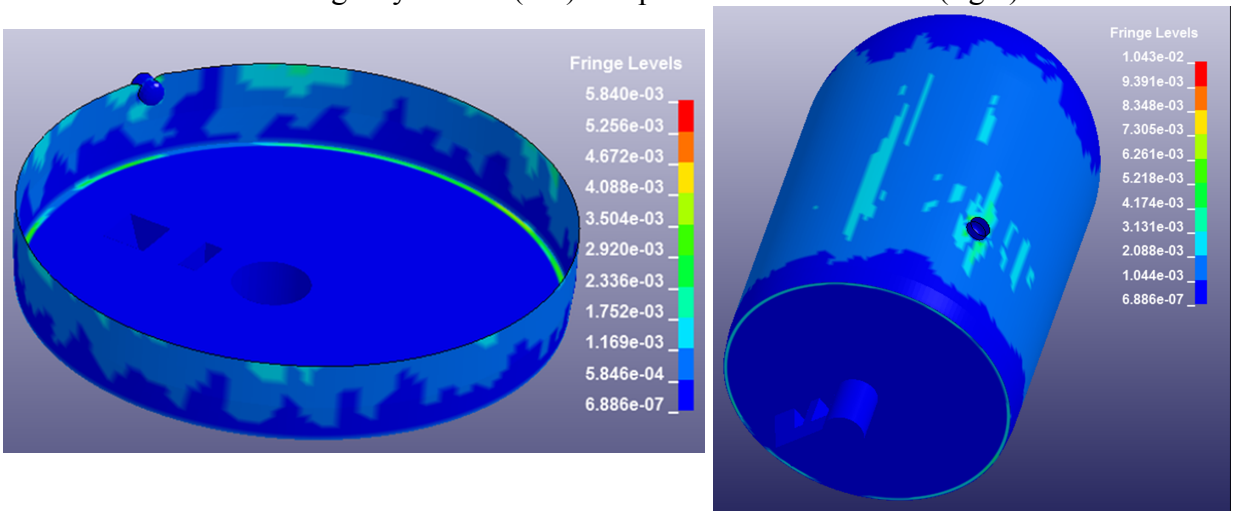

Figure 5: Maximum principal strains at 0.90MPa (131psig) in the liner at the wall-basemat junction: inside view (left) and bottom view (right) (strain scales are different in each picture)

Containment Hatch, Emergency Airlock and Personal Airlock – Leakage at these locations would start at an internal pressure of about 0.83MPa (120psig). The total leakage area would increase rapidly as the internal pressure increases, reaching values greater than 93 cm^2 ($0.1ft^2$) at about 0.86MPa (124psig) and values in the range of 280 to 930 cm^2 ($0.3 - 1.0ft^2$)

between 0.87 and 0.88MPa (126 and 128psig). Most of the leakage area would be in the containment hatch region. According to the analysis, the liner tears would spread and the containment leakage area would increase quickly as the internal pressures increase above 0.88 MPa (128psig).

Containment Wall and Basemat Junction – The leakage area at these locations would increase rapidly as the internal pressure increases, reaching values greater than 93cm^2 (0.1ft^2) at about 0.9MPa (131psi) and values in the range of 280 to 930cm^2 (0.3 - 1.0ft^2) between 0.90 and 0.92MPa (131 and 134psig). Examination of maximum principal strain contours (tensile strains) in this region, indicate that cracks would develop at the base of the wall and basemat slab and that the likely leakage path would be through cracks in the concrete extending to the tendon galleries under the containment wall. The outermost part of the base of the containment wall would still be subjected to compressive stresses as a result of local bending of the wall thus making the path to the tendon galleries more likely than the path at the base of the walls.

Containment Failure Pressure Capacity

The analysis results also provide an estimate of the failure pressure capacity of the containment as measured by either the pressure at which a certain threshold strain would be widespread in the hoop tendons or the pressure at which shear failure at the junction of the containment wall to the foundation slab (basemat) might initiate. Here, the threshold strain for the hoop tendons is taken to be 1% which is generally consistent with Regulatory Guide 1.216 [NRC, 2010]. Internal pressures corresponding to the containment failure capacity are possible only if the rate of internal pressurization from the severe accident exceeds the leakage rate from tearing of the liner.

Tendon Strains – Tensile strains of about 1-percent are widespread in the hoop tendons at internal pressures between about 1.10 to 1.16MPa (159 to 168psig) with a central estimate of about 1.13MPa (164psig) as shown in Figure 6. At these pressures and strains, the leakage area would be expected to exceed 930cm^2 (1ft^2) and be of the order of about 10ft^2.

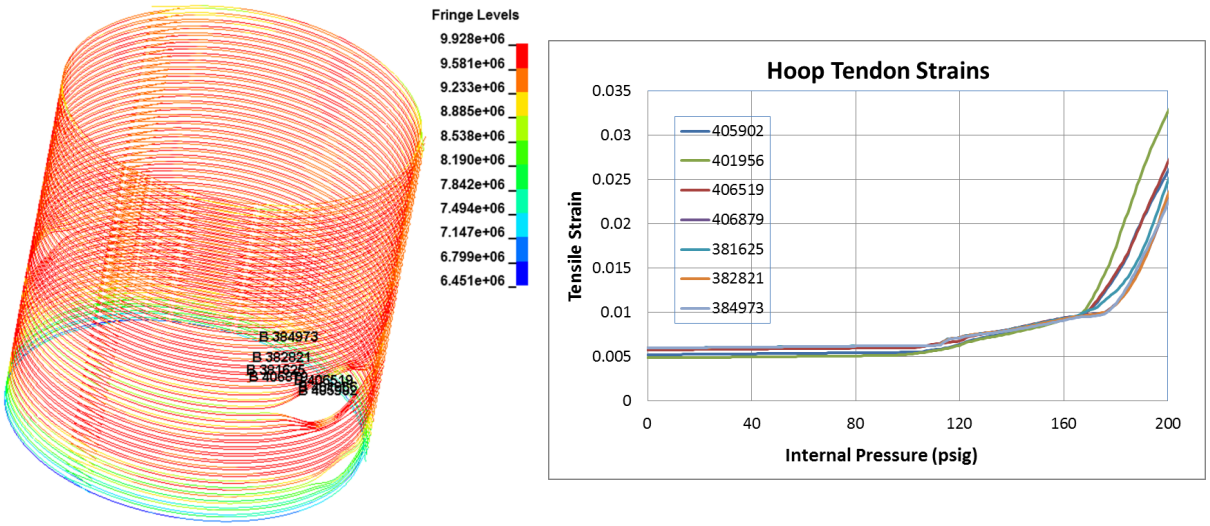

Figure 6. Forces (left) and strains (right) on hoop tendons (Forces are in newtons and the force at 1-percent strain is 9.7×10^6newtons (2.2×10^6lbf))

Shear at the wall-basemat junction – Examination of contours of maximum principal strains in the basemat indicate that cracking at the wall-basemat junction would extend to the basemat and might reach the bottom of the basemat (ceiling of the tendon gallery) at pressures in the range of 0.90 to 0.92 MPa (131 to 134psig). However, these results are not conclusive in that they do no clearly indicate that a connected network of cracks would clearly develop through the basemat. Furthermore, at these pressures, tensile strains (and crack widths) at the bottom of the basemat are still small and although they could provide a leakage path to the tendon gallery they are not expected to correspond to a shear failure. Bands of maximum tensile strains equal to about 0.5% (0.005) develop through the basemat at internal pressures in the range of 1.16 to 1.20 MPa (168 to 174psig) as illustrated in Figure 7 for the basemat under a concrete buttress. These bands are taken as an indication of shear failure initiation through the concrete basemat near the wall-basemat junction.

The results of the analysis indicate containment failure capacities at internal pressures of about 1.10MPa (159psig) for the containment wall when strains in the hoop tendons reach a value of about 1.0%, and at about 1.16MPa (168psig) for shear failure at the wall-basemat junction. These pressures could only be achieved for a rate of internal pressurization of the containment greater than the leakage rate that is expected to start at lower pressures. These containment failure capacities do not represent internal pressures corresponding to catastrophic failure of the containment but pressures at which the containment wall deformations would increase rapidly as the internal pressure increases.

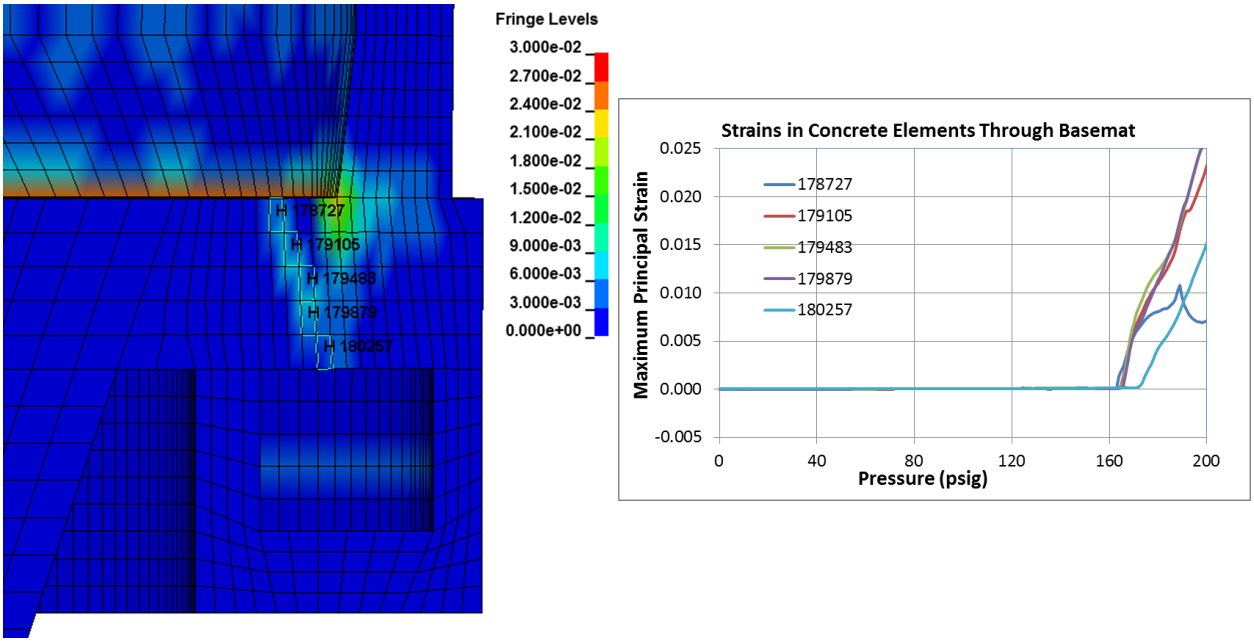

Figure 7: Maximum principal strain contours (left) and time-histories in concrete elements through the basemat (right)

The modeling approach provides promising results that are generally consistent with results that would be expected based on insights obtained from prior containment testing and analyses [HES03], [HES06]. Execution of the finite element analysis on a dedicated personal computer with 12 processors took about 14.5 hours. This seems to be sufficiently fast so that sensitivity analysis and uncertainty analysis with, for example, Latin Hypercube statistical simulation are feasible with this modeling and analysis.

Conclusions

This paper describes the modeling and results of a three-dimensional finite element analysis of a post-tensioned concrete containment with ungrouted tendons for beyond-design basis internal pressurization. Goals for the analysis include illustrating results that would inform Level 2 probabilistic risk assessments and assessing modern modeling and analysis techniques. The modeling approach provides promising results that are generally consistent with results that would be expected based on insights obtained from prior containment testing and analyses. The calculations with this modeling and explicit analysis are sufficiently fast so that sensitivity

analysis and uncertainty analysis with, for example, Latin Hypercube statistical simulation is feasible.

References

[NRC10] Nuclear Regulatory Commission, "Containment Structural Integrity Evaluation For Internal Pressure Loadings Above Design Basis Pressure," *Regulatory Guide 1.216*, U.S. Nuclear Regulatory Commission, Rockville, MD, USA.

[LST13] Livermore Software Technology Corporation, "LSDYNA Keyword User's Manual," Version R 7.0, Livermore Technology Software Corporation (LSTC), Livermore, California, USA, 2013.

[CHE96] Cherry, J. L., "Analyses of Containment Structures with Corrosion Damage," *Pressure Vessel and Piping,* Vol. 343, Development, Validation, and Application of Inelastic Methods for Structural Analysis and Design, ASME, R. F. Sammazaro and D. J. Ammerman, Editors, pp. 15-23, Atlanta, GA, 1996.

[TAN95] Tang, H.T., R.A. Dameron, and Y.R. Rashid, "Probabilistic Evaluation of Concrete Containment Capacity for Beyond Design Basis Internal Pressures," *Nuclear Engineering and Design*, Vol. 157, pp. 455-467.

[SPE06] Spencer, B.W., Petti, J.P., Kunsman, S.M., Graves, H.L., "Risk-Informed Assessment of Degraded Containment Vessels," *NUREG/CR-6920* (SAN2006-3772P), U.S. Nuclear Regulatory Commission, Rockville, MD, USA, November, 2006.

[PET13] 2013 Petti, J.P., D. A. Kalinich, J. Jun, K.C. Wagner, "Effects of Degradation on the Severe Accident Consequences for a PWR Plant with a Reinforced Concrete Containment Vessel," *NUREG/CR-7149* (SAND2009-6323P), U.S. Nuclear Regulatory Commission, Rockville, MD, USA, June, 2013.

[CHE01] Cherry, J.L. and J.A. Smith, "Capacity of Steel and Concrete Containment Vessels with Corrosion Damage," *NUREG/CR-6706* (SAND2000-1735), U.S. Nuclear Regulatory Commission, Rockville, MD, USA, February, 2001.

[HES03] Hessheimer, M.F., Klamerus, E.W, Lambert, L.D., Rightley, G.S., Dameron, R.A., "Overpressurization Test of a 1:4-Scale Prestressed Concrete Containment Vessel Model," *NUREG/CR-6810* (SAND2003-0840P), U.S. Nuclear Regulatory Commission, Rockville, MD, USA, March, 2003.

[HES06] Hessheimer, M.F., Dameron, R.A., Sheikh, A., "Containment Integrity Research at Sandia National Laboratories," *NUREG/CR-6906* (SAN2006-2274P), U.S. Nuclear Regulatory Commission, Rockville, MD, USA, July, 2006.

Disclaimer

This paper was prepared under the auspices of an agency of the U.S. Government. Neither the U.S. Government nor any agency thereof, nor any of their employees, makes any warranty, expressed or implied, or assumes any legal liability or responsibility for any third party's use, or the results of such use, of any information, apparatus, product, or process disclosed in this paper, or represents that its use by such third party would not infringe privately owned rights. The views expressed in this paper are not necessarily those of the U.S. Nuclear Regulatory Commission.